Analysis of MMIC Structures Using an Efficient Iterative Approach

CHI HOU CHAN, MEMBER, IEEE, AND RAJ MITTRA, FELLOW, IEEE

Abstract — **In this paper a class of two- and three-dimensional monolithic microwave integrated circuit (MMIC) structures is theoretically analyzed using an efficient iterative technique. The transfer-matrix approach to constructing the spectral Green's functions of multilayered structures is adopted. Discretization of the continuous functions and exploitation of the periodicity of the MMIC structures enclosed by side walls lead to a discrete convolution operation, which can be carried out numerically efficiently using the FFT algorithm. The spectral Green's functions are modified for both the periodic and aperiodic structures to improve the numerical efficiency of the iterative algorithm. Numerical results are presented and compared with available data.**

I. Introduction

PLANAR MICROSTRIP structures used in MMIC design, such as multiconductor transmission lines, patches, and discontinuities, have been extensively analyzed in the past two decades by several authors using the quasi-TEM approximation. This approximation avoids extensive numerical calculations in the full-wave analysis, and yet provides useful results sufficiently accurate for practical applications up to a few gigahertz.

Coupled planar transmission lines have been analyzed using the following approaches: conformal mapping [1]; dielectric Green's function method [2]; variational method [3]; and Galerkin method in the spectral domain [4]. Multiconductor transmission lines have been treated in [5] and, more recently, in [6] and [7]. There is no theoretical limit to the number of dielectric layers or conducting lines in these formulations; however, they require either the solution of a large matrix equation or extensive analytical or numerical calculations.

Finite-sized or lumped circuit elements such as microstrip patches are also commonly used in MMIC's. Capacitances of square and circular patches have been calculated in [8]–[11]. In the above papers, accurate and rapid solutions have been obtained using the spectral Gelerkin procedure with a set of prechosen basis functions. However, the choice of basis functions for an arbitrarily shaped patch is often not readily available.

For computer-aided design of MMIC's, microstrip discontinuities are often represented by equivalent circuit parameters [12], [13]. One of these parameters, the equivalent capacitance of a microstrip discontinuity, is calculated by discretizing the excess charge distribution [13] in the discontinuity and its surrounding regions using subdomain basis functions, e.g., square pulses, and solving for the unknown amplitude of these pulses with the standard moment method procedure. However, the matrix equation resulting from an application of this approach can be very large and its elements often require an excessive computational time.

Recently, an iterative scheme based upon the minimization of the integrated square error has been developed by van den Berg [14]. It has been applied to the problem of analyzing the electric-field problem of an interdigital transducer in a multilayered structure [15] and to a class of multiconductor cylindrical transmission lines [16]. In this iterative procedure, the large matrix storage requirement is alleviated and numerical efficiency is obtained by using the fast Fourier transform algorithm (FTT).

In this paper, a variety of two- and three-dimensional MMIC structures are analyzed using the iterative procedure described in [14, table V] by van den Berg for the case where the number of dielectric layers in these MMIC structures is arbitrary. It is assumed that the principal axes of the permittivity tensor and the conductivity tensor coincide and that only the diagonal terms are nonzero. The choice of basis and testing functions, as well as the numerical treatment of the Green's functions that improves the numerical efficiency of the algorithm, is discussed. In order to apply the FFT, all the dimensions of the MMIC structures are chosen to be multiples of the discretization value Δx or Δy. Numerical results for each of the MMIC structures discussed in this paper are presented and compared with published data, when available.

II. Outline of the Theoretical Procedures

The general configuration to be investigated is shown in Fig. 1(a) and (b) with the permittivity tensor ϵ and conductivity tensor σ given by

$$\epsilon = \begin{pmatrix} \epsilon_x & 0 & 0 \\ 0 & \epsilon_y & 0 \\ 0 & 0 & \epsilon_z \end{pmatrix} \qquad \sigma = \begin{pmatrix} \sigma_x & 0 & 0 \\ 0 & \sigma_y & 0 \\ 0 & 0 & \sigma_z \end{pmatrix}. \tag{1}$$

We define the regions that coincide with the conducting strips as the domain D of the problem and the complementary region as the range R. In this study, the strips are assumed to be infinitely thin, although the extension to the

Manuscript received February 19, 1987; revised July 27, 1987. This work was supported in part by the Army Research Office under Grant DAAG29-85-K-0183.

The authors are with the Electromagnetic Communication Laboratory, Department of Electrical and Computer Engineering, University of Illinois, Urbana, IL 61801.

IEEE Log Number 8717585.

0018-9480/88/0100-0096$01.00 ©1988 IEEE

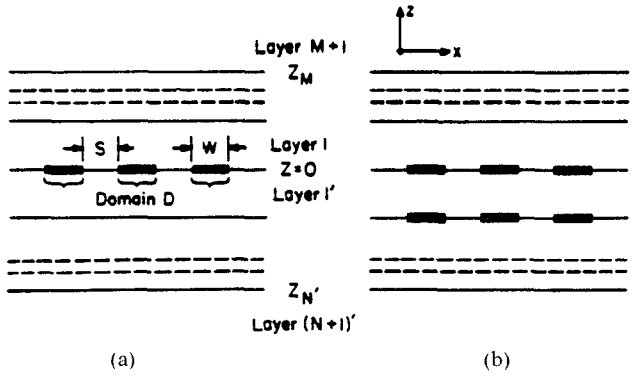

Fig 1. The general multilayered MMIC structures. (a) One layer of strips. (b) Two layers of strips.

finite thickness strips can be found elsewhere [3], [16]. Under the quasi-TEM approximation, we may assume $\nabla \times \vec{E} = 0$. With the factor $e^{j\omega t}$ suppressed, the electric field $\vec{E}$ and the electric potential V are related by

$$\vec{E} = -\nabla V. \tag{2}$$

The electric field, in turn, is related to the current density as follows:

$$\vec{J} = (\sigma + j\omega\epsilon)\cdot\vec{E}. \tag{3}$$

Using the continuity equation $\nabla \cdot \vec{J} = 0$ in conjunction with (3), we obtain a differential equation satisfied by the electric potential V for each of the layers:

$$\nabla \cdot [(\sigma + j\omega\epsilon)\cdot\nabla V] = 0. \tag{4}$$

The Green's function for the problem can be constructed from the solution of this differential equation subject to appropriate boundary conditions. The boundary conditions for these MMIC structures are the continuity of the electric potential V across any interface, constant voltage excitation U on the conducting strips or patches, and a nonzero current density $\vec{J}$ confined to the domain D. Once the Green's function is derived, we can simply cast the problem into one of solving the integral equation

$$U(s) = \int_D G(s', s)(j\omega\rho_s(s'))\, ds' \tag{5}$$

where G is the Green's function in the spatial domain and ρ_s is the unknown surface charge distribution. The term $j\omega\rho_s$ replaces the role of the current density $\vec{J}$. The total charges on the conductors are obtained by integrating ρ_s in the domain D. Once the total charge on each of the conducting strips or patches is known, the various design parameters of the MMIC structures, e.g., the capacitance, inductance, effective dielectric constant, and the characteristic impedance, can be readily obtained [16].

III. The Spectral Green's Functions

Prior to formulating the integral equation using the spectral domain approach, we need to derive the spectral Green's function for the geometry under consideration. The spectral Green's function can be derived by solving Laplace's equation together with the appropriate boundary conditions of the structure [3], [16]. However, a new derivation of the Green's function is required whenever an additional layer of dielectric is added to the structure. Two approaches, which are quite similar to each other, have recently been introduced for deriving the spectral Green's functions for a multilayered structure. A simple recurrence formula has been presented in [17] and a transfer-matrix formulation has been discussed in [15]. In both of these approaches, an additional dielectric layer only results in an extra 2×2 matrix multiplication in the transfer matrix or the recurrence formula; hence, these approaches are well suited for computer-aided design of MMIC's. In this paper, we adopt the transfer-matrix formulation of [15], because this procedure is simple to follow.

The details of deriving the spectral Green's function for the structure in Fig. 1(a) using the transfer-matrix approach can be found in [15], and only the final result is included here for completeness. The derivation procedure can be readily extended to the structure consisting of two or more layers of strips by enforcing the additional boundary conditions on the interfaces at which the extra layers of strips are located. The spectral Green's function for the structure in Fig. 1(b), which has two layers of strips, is presented here with the details of the derivation omitted.

The spectral Green's function for the convolution integral of (5), employed to analyze the structure of Fig. 1(a), is given in [15]. It reads

$$\tilde{G}(\alpha) = \frac{1}{Y_1^+(\alpha) + Y_{1'}^-(\alpha)} \tag{6}$$

where

$$Y_1^+(\alpha) = \frac{T_{1\to M}^{(2,1)} + Y_{m+1}T_{1\to M}^{(2,2)}}{T_{1\to M}^{(1,1)} + Y_{M+1}T_{1\to M}^{(1,2)}} \tag{7a}$$

and

$$Y_{1'}^-(\alpha) = -\frac{T_{1'\to N'}^{(2,1)} - Y_{(N+1)}T_{1'\to N'}^{(2,2)}}{T_{1'\to N'}^{(1,1)} - Y_{(N+1)'}T_{1'\to N'}^{(1,2)}}. \tag{7b}$$

If the top layer of the structure is shielded, i.e., the plane at $z = z_M$ is grounded, the expression for $Y_1^+(\alpha)$ is modified as follows:

$$Y_1^+(\alpha) = \frac{T_{1\to M}^{(2,2)}}{T_{1\to M}^{(1,2)}}. \tag{8a}$$

Similarly, if the plane at $z = z_{N'}$ is grounded, we have

$$Y_{1'}^-(\alpha) = \frac{T_{1'\to N'}^{(2,2)}}{T_{1'\to N'}^{(1,2)}}. \tag{8b}$$

The transfer matrix T appearing in the above expression is defined as follows:

$$\begin{bmatrix} T_{1\to M}^{(1,1)} & T_{1\to M}^{(1,2)} \\ T_{1\to M}^{(2,1)} & T_{1\to M}^{(2,2)} \end{bmatrix} = \prod_{m=1}^{M} [T_m(\alpha, z_{m-1} - z_m)] \tag{9}$$

where

$$T_m(\alpha, z) = \begin{bmatrix} \cosh\gamma_m z & -Y_m^{-1}\sinh\gamma_m z \\ -Y_m \sinh\gamma_m z & \cosh\gamma_m z \end{bmatrix} \quad (10)$$

$$\gamma_m(\alpha) = |\alpha|(\kappa_{x,m}/\kappa_{z,m})^{1/2} \quad (11)$$

$$Y_m(\alpha) = j\omega|\alpha|(\kappa_{x,m}\cdot\kappa_{z,m})^{1/2} \quad (12)$$

$$\kappa_{x,m} = \epsilon_{x,m} + \sigma_{x,m}/j\omega \quad (13a)$$

$$\kappa_{z,m} = \epsilon_{z,m} + \sigma_{z,m}/j\omega \quad (13b)$$

and the square roots are defined as $\mathrm{Re}(\cdots)^{1/2} \geqslant 0$. Expressions similar to (9) to (13) can readily be obtained for the layers below $z = 0$ by replacing 1, M, and m by 1′, N', and n' in (9) to (13), respectively.

Following the derivation given in [15], and enforcing the boundary conditions on the two layers of strips, we obtain the spectral Green's function for the structure shown n Fig. 1(b). It is given by

$$\tilde{G}(\alpha) = \begin{bmatrix} \tilde{G}_{11}(\alpha) & \tilde{G}_{12}(\alpha) \\ \tilde{G}_{21}(\alpha) & \tilde{G}_{22}(\alpha) \end{bmatrix}$$

$$= \begin{bmatrix} \dfrac{-Y_{2'}^{-} + Y_{1'}\coth\gamma_{1'}d}{C(\alpha)} & \dfrac{Y_{1'}/\sinh\gamma_{1'}d}{C(\alpha)} \\ \dfrac{Y_{1'}/\sinh\gamma_{1'}d}{C(\alpha)} & \dfrac{Y_1^{+} + Y_{1'}\coth\gamma_{1'}d}{C(\alpha)} \end{bmatrix} \quad (14)$$

where

$$C(\alpha) = \left[-Y_1^{+}Y_{2'}^{-} + (Y_1^{+} - Y_{2'}^{-})Y_{1'}\coth\gamma_{1'}d + Y_{1'}^2\right]. \quad (15)$$

Note that the spectral Green's function is a 2×2 matrix because of the coupling between the two layers of strips.

It is preferable to use the spectral Green's function given in (6) rather than the spatial one, because we can efficiently compute the convolution integral in (5) via the FFT. In the next section, we go on to discuss some numerical aspects for solving (5) for some aperiodic and periodic problems arising in MMIC design. Some of these numerical aspects have been discussed by Peterson [18] and Chan and Mittra [19].

IV. Numerical Considerations for Applying the FFT to Periodic and Aperiodic Problems

Strictly speaking, the FFT algorithm, which is discrete and circular in nature, is directly applicable for analyzing periodic geometries. However, it can be still used to address aperiodic problems if they are approximated by introducing two electric side walls that are sufficiently removed from the center strips. Additional approximations, which we will discuss in the latter part of this section, can be used to reduce the size of the FFT for the aperiodic case, and to make the iterative procedure numerically efficient. A discussion of the numerical treatments for the periodic and aperiodic structures is given below.

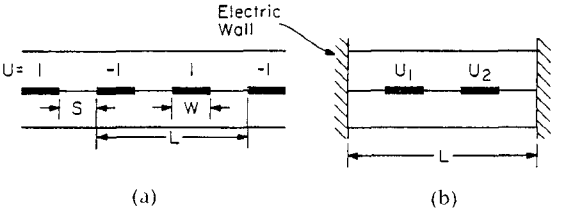

Fig. 2. Periodic MMIC structures. (a) Periodic structure without side walls. (b) Periodic structure with two side walls.

A. Periodic Structures

The spectral Green's function given in Section III can be employed for periodic structures, although special numerical treatment is necessary to apply the FFT to this Green's function because of its infinite support. To demonstrate how the FFT can be applied correctly, we consider the periodic structures shown in Fig. 2(a) and (b). The periodic cell of Fig. 2(a), or the region between the two side walls in Fig. 2(b), both of which have the dimension L, is discretized into N subregions, where $N = 2^m$. Assuming that the potential U and the surface charge density ρ_s are approximately constant over the subregions, U and ρ_s can be expressed as a sum of rectangular pulse basis functions with known amplitudes $U(n)$ and unknown amplitudes $\rho_s(n)$, respectively. After some manipulation, the convolution integral in (5) can then be rewritten as

$$\Theta[U(n\Delta x)]$$
$$= \Theta\left[\mathrm{F}^{-1}\left\{\tilde{G}(\alpha)\tilde{S}(\alpha)\left(\mathrm{FFT}(\rho_s(n))*\delta(n+mN)\right)\right\}\right] \quad (16)$$

where Θ is a truncation function with value equal to 1 when $n\Delta x$ is inside the domain D and zero otherwise. Similarly, $\rho_s(n)$ is nonzero only if $n\Delta x \in D$. F^{-1} represents the inverse Fourier transform operation and the FFT is defined from $-N/2$ to $N/2-1$; Δx and α are equal to L/N and $(n+mN)2\pi/L$ with $-\infty < m < \infty$, respectively; $\tilde{S}(\alpha) = \sin(\alpha)/\alpha$ is the Fourier transform of the rectangular pulse. The asterisk in (16) represents a convolution operator. The support of the inverse Fourier transform in (16) is still infinite; however, this could be overcome by applying the Galerkin procedure, i.e., multiplying both sides by the rectangular pulses and integrating over the corresponding subregions. We then obtain

$$\Theta[U(n)] = \Theta\left[\mathrm{FFT}^{-1}\left\{\tilde{G}'(\alpha)\,\mathrm{FFT}(\rho_s(n))\right\}\right] \quad (17)$$

where

$$\tilde{G}'(\alpha) = \sum_{m=-\infty}^{m+\infty} \tilde{G}(\alpha')\tilde{S}(\alpha')\tilde{S}^{*}(\alpha'). \quad (18)$$

The asterisk represents the complex conjugate operation and $\alpha' = (n+mN)2\pi/L$. The truncation on m depends on how fast the product of the spectral Green's function and the magnitude square of the Fourier transform of the basis function decays away from $\alpha = 0$. The charge density distribution in (17) of the periodic structures can readily be solved for via the iterative algorithm outlined in [14].

The procedure outlined above is applicable only to periodic structures, and a different approximation scheme is required for the aperiodic case. This is described in the following subsection.

B. Aperiodic Structures

An aperiodic structure can be approximated by a periodic one by introducing two side walls far away from the conducting strips. This is accomplished by letting L in Fig. 2(b) to be sufficiently large, such that the side walls do not have a significant effect on the electric potential around the strips. We can then follow the same procedure as in the periodic case discussed above. However, this requires us to use a large value of N and increases the computational time significantly. We show below how we can circumvent the problem by further approximating the Green's function such that a much smaller N can be used without compromising the accuracy of the computation.

The Green's function can be approximated by assuming that it is constant over the individual subregions in the spatial domain. Let the potential U and the surface charge density ρ_s be discretized, once again using rectangular pulse basis functions. From signal processing theory, we can show that the convolution integral in (5) can be carried out with a $(2M-1)$-point FFT, where M is the number of subregions from the left edge of the leftmost strip to the right edge of the rightmost strip. If we use a radix-2 N-point FFT, we should choose the minimum N such that $N > (2M-1)$. Using this criterion, the spatial Green's function can be obtained from the spectral one via a numerical transform.

The spectral Green's function in Section III is sampled at the values of $2\pi n/NN\Delta x$, where $-NN/2 \leqslant n \leqslant NN/2 - 1$ and $NN\Delta = L$. Typically, we choose $NN = 1024$ for a one-dimensional problem and $NN \times NN = 512 \times 512$ for a two-dimensional one. These data points are inversely Fourier transformed into the spatial domain by using an NN-point FFT. Although NN is large, this FFT operation need be carried out only once. The approximated spatial-domain Green's function is then truncated such that only those terms within the range $-NN/2 \ll -N/2 \leqslant n \leqslant N/2-1 \ll NN/2-1$ are retained. It is noted that an equivalent procedure is discussed in [15], except all the NN terms were retained there.

To illustrate the versatility of the iterative approach in solving (5) for the periodic and aperiodic MMIC structures under the approximation mentioned above, we will consider both the two- and three-dimensional problems in the following sections.

V. Two-Dimensional Problems

Planar transmission lines find many applications in MMIC design as well as in microelectronic packaging. These transmission lines are usually assumed to have infinite extension in the y direction, as shown in Fig. 1. In this section, we will consider two examples of these transmission lines, viz., a broadside, edge-coupled symmetric strip transmission line which is a periodic problem and a multiconductor planar transmission line in a piezoelectric substrate—an aperiodic one. Although not discussed here, many other types of planar transmission lines, e.g., microstrip, buried microstrip, and strip lines, can also be analyzed by utilizing the novel representation of the spectral Green's function.

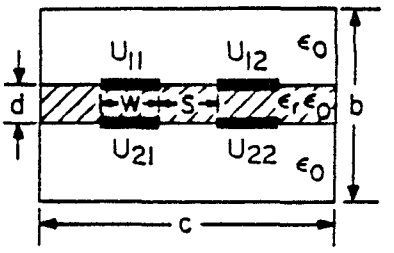

Fig. 3. A broadside, edge-coupled, symmetric strip transmission line.

A. Broadside, Edge-Coupled, Symmetric Strip Transmission Line

Recently, considerable interest has been shown in using a broadside, edge-coupled, symmetric strip transmission line in MMIC's as a basic building block for directional couplers, filters, and broad-band mixers [20], [21]. A schematic diagram of one of these transmission lines is depicted in Fig. 3. This structure can support four propagating modes referred to as

1) even–even mode (ee): $U_{11} = U_{12} = U_{21} = U_{22}$
2) even–odd mode (eo): $U_{11} = U_{12} = -U_{21} = -U_{22}$
3) odd–even mode (oe): $U_{11} = -U_{12} = U_{21} = -U_{22}$
4) odd–odd mode (oo): $U_{11} = -U_{12} = -U_{21} = U_{22}$.

Equation (16) can be solved iteratively using the Green's function derived in (14). Due to the symmetry of the problem, the characteristic impedance (Z) and the effective dielectric constant (ϵ_{eff}) can be written in terms of the total charge Q on one of the lines as

$$Z = \frac{Z_0}{(QQ_0)^{1/2}} \tag{19}$$

$$\epsilon_{\text{eff}} = \frac{Q}{Q_0} \tag{20}$$

where Q and Q_0 are the total charge on one of the strips with and without the dielectric, respectively, and Z_0 is the characteristic impedance in free space. The total charge on the strip is obtained by integrating the charge density distribution across the strip after solving (16).

Although this structure is symmetric, the iterative algorithm is written such that each of the strip's widths w as well as the separation between the strips s can be different. Some numerical results on the effective dielectric constant of the structure shown in Fig. 3 will be given in Section VII.

B. Multiconductor Planar Transmission Lines in a Piezoelectric Substrate

To illustrate the numerical efficiency achieved by applying the numerical treatment of the Green's function for the

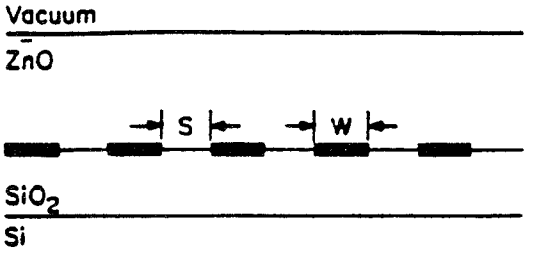

Fig 4 A multiconductor planar transmission line in a piezoelectric substrate

aperiodic structure, we consider the multiconductor planar transmission lines in a piezoelectric substrate shown in Fig. 4. van den Berg and his associates have successfully applied iterative procedures to solve the electric-field problem of an interdigital transducer in a multilayered structure [15]. In [15], the conducting strips are excited such that the net electric current in the configuration vanishes. Furthermore, integration of the potential along the interface at which the strips are located also yields zero. However, in a general transmission line structure, the voltage excitation applied to the strips can be arbitrary. This is the case, for instance, when one is interested in computing the Maxwell capacitance matrix of an N-line configuration and needs to solve (5) N times for N independent sets of excitations. To simulate the infinite domain in which the conducting strips are located, a period of 50 times the width of one strip is used in [15]. In Section VII, we will demonstrate how the numerical treatment discussed in Section IV reduces the size of the period actually required.

VI. Three-Dimensional Problems

When the width of the transmission line in Fig. 1 varies along the length of the line, or the line has a finite length, the two-dimensional problem becomes three-dimensional in nature. The spectral Green's function given in Section III can be modified to treat the three-dimensional problem. However, to keep the modification simple, we assume that the diagonal elements of the permittivity tensor in (1) are all equal and set all the elements of the conductivity tensor in (2) equal to zero. The three-dimensional structures discussed in this section are aperiodic and, in order to apply the FFT, we need to introduce four electric side walls sufficiently far away from the conducting patches or discontinuities under consideration. The separations of the side walls in the x- and y directions are designated as L_x and L_y, respectively. To obtain the three-dimensional spectral Green's function $\tilde{G}(\beta, \zeta)$, we simply replace the parameter α in (6) and (14) with $\sqrt{\beta^2+\zeta^2}$, where $\beta = n2\pi/L_x$ and $\zeta = m2\pi/L_y$. Similarly, the one-dimensional FFT becomes two-dimensional in solving (5). The truncation of the spatial Green's function in the y direction follows the same criterion for the one in the x direction. Only some illustrative three-dimensional structures are discussed in this section. Extension to treat many other structures, e.g., two arbitrarily shaped coupled patches which lie on the same plane or are separated by a dielectric slab, is straightforward.

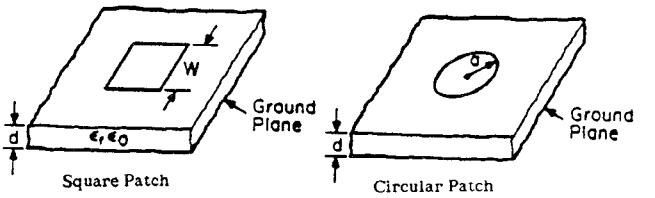

Fig. 5. A square and a circular microstrip patches

A. Microstrip Patches as Lumped Circuit Elements

In MMIC's, many finite-sized or lumped elements are employed to realize the desired functional devices. Hence the analysis of these finite-sized elements is of interest. Among these finite elements, square and circular patches (shown in Fig. 5) have been analyzed more frequently than the others because the charge densities on these structure can be expanded in terms of a set of entire domain basis functions [8]–[11] with certain special properties, viz., analytical Fourier transformability, built-in edge condition for the charge distributions, and ability to generate asymptotic formulas [11]. However, for an arbitrarily shaped patch, the choice of these entire domain basis functions is not readily available and this prompts us to use subdomain basis functions, such as the rectangular pulses discussed in Section IV.

In order to employ the rectangular pulse type of basis functions to solve (5) and to apply the numerical treatment of the Green's function discussed in Section IV, we need to carry out an inverse FFT on a large-sized array sampled on the two-dimensional spectral Green's function. Fortunately, in a typical fabrication scenario, the thickness and the permittivity of the dielectric are fixed at certain prechosen values. Hence, for this type of situation, we need to carry out the inverse FFT only once and store the truncated spatial Green's function, thus generated, as a data base for MMIC designs.

Once the spatial Green's function has been obtained, (5) can be solved with the potential U on the patch set equal to 1 V. The capacitance of the patch is then given by

$$C = \int_D \rho_s(s)\, ds. \tag{21}$$

Numerical results for the normalized capacitance will be presented in Section VII for a square and a circular patch. Because of discretization using rectangular pulses, the periphery of the circular patch, or of any other arbitrary shape, can only be approximated in a piecewise manner.

B. Equivalent Capacitances for Discontinuities in Microstrip Lines and at the Crossing of Orthogonal Strip Lines

Abrupt change of line width in planar transmission lines is often unavoidable for printed circuit routing. Sometimes, such a discontinuity is even introduced deliberately to realize an inductance or a capacitance. Another form of discontinuity is found in the vicinity of a crossing between two orthogonal strip lines, where there exists a strong coupling between these strip lines. Both of these discontinuities, viz., the change of width and the cross coupling

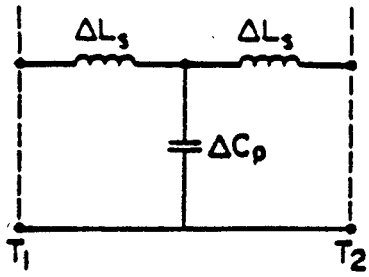

Fig. 6. The equivalent circuit for microstrip discontinuities.

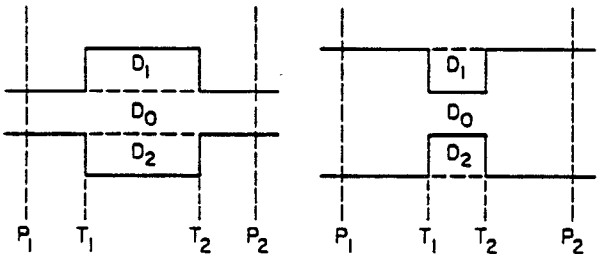

Fig. 7. Double step microstrip discontinuities.

between two striplines, can be characterized by an equivalent circuit of the type shown in Fig. 6. In this paper, we will only address the problem of computing the equivalent capacitance, except to mention that a similar procedure can be used to derive the equivalent inductance of the discontinuity.

To find the equivalent capacitance of a double step discontinuity, Kitazawa [22] has formulated the problem of determining the excess charge density on the transmission line in the presence of the discontinuity. The same formulation is employed herein for the first type of discontinuity problem and is later extended to characterize the disturbance of surface charge density near the crossing of two orthogonal striplines.

1) Microstrip Discontinuities: Two different microstrip discontinuities are shown in Fig. 7(a) and (b); D_0 denotes the regions with uniform width, whereas D_1 and D_2 denote the irregular regions. To characterize the discontinuity, we need to find, as a first step, the charge density ρ_{s0} on the uniform line denoted by D_0 for a 1 V excitation, using the procedures outlined in Section V. We define the excess charge density $\rho_{s\,\mathrm{ex}}$ as the difference between the charge density of the structure D and that of the uniform structure D_0 when both are excited by 1 V; it should be noted that $\rho_{s\,\mathrm{ex}}$ is only defined on D. After some manipulation, we have

$$\phi_{\mathrm{ex}} = \int_D G(j\omega\rho_{s\,\mathrm{ex}})\, ds \tag{22}$$

where for the discontinuity in Fig. 7(a)

$$\phi_{\mathrm{ex}} = \begin{cases} 0 & \text{on } D_0 \\ 1 - \int_{D_0} G(j\omega\rho_{s0})\, ds & \text{on } D_1 \text{ and } D_2 \end{cases} \tag{23}$$

and for the discontinuity in Fig. 7(b)

$$\phi_{\mathrm{ex}} = \int_{D_1, D_2} G(j\omega)(\rho_{s1} + \rho_{s2})\, ds. \tag{24}$$

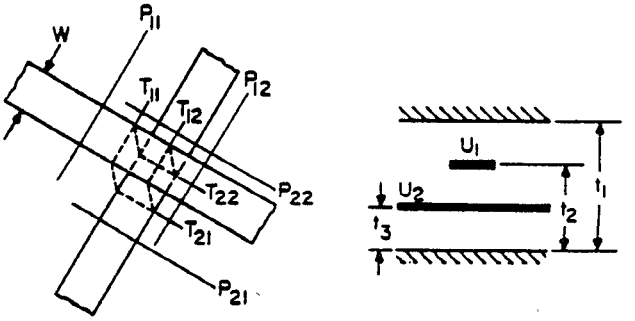

Fig. 8. Two orthogonal strip lines.

The densities ρ_{s1} and ρ_{s2} are ρ_{s0} in regions D_1 and D_2, respectively. The excess charge is essentially negligible, beyond a distance approximately equal to the actual line width away from the discontinuity [13]. Hence, the domain of integration in (22) can be limited to the region bounded by the planes P_1 and P_2 indicated in Fig. 7.

Once the excess charge density has been solved for, the equivalent capacitance ΔC can be defined as

$$\Delta C = \int_{S_1} \rho_{s\,\mathrm{ex}}\, ds + \int_{S_2} \rho_{s0}\, ds \tag{25}$$

where S_1 and S_2 are the regions bounded by the planes P_1, P_2 and T_1, T_2, respectively. Numerical results of the normalized equivalent capacitance for double-step discontinuities will be presented in Section VII.

2) Crossing of Two Orthogonal Strip Lines: The surface current and charge density on a strip line, near the vicinity of its crossing with another stripline which is orthogonally placed above or below it, is expected to be a perturbation from those on an isolated strip line. The disturbance of the surface current or the charge density on the strip line can also be characterized by an equivalent capacitance. Since either an even ($U_1 = U_2 = 1$ V) or odd ($U_1 = -U_2 = 1$ V) excitation can be applied to the two orthogonal strip lines depicted in Fig. 8, we need to compute both the even and odd equivalent capacitances for the strip lines.

Excess charge densities $\rho_{s\,\mathrm{ex}1}$ and $\rho_{s\,\mathrm{ex}2}$ can be defined for the two orthogonal strip lines similar to the one for the microstrip discontinuity. These excess charge densities satisfy the following equations:

$$\phi_{\mathrm{ex}1} = \int_{D_1} G_{11}\rho_{s\,\mathrm{ex}1}\, ds + \int_{D_2} G_{12}\rho_{s\,\mathrm{ex}2}\, ds \qquad \text{on } D_1 \tag{26a}$$

$$\phi_{\mathrm{ex}2} = \int_{S_1} G_{21}\rho_{s\,\mathrm{ex}1}\, ds + \int_{D_2} G_{22}\rho_{s\,\mathrm{ex}2}\, ds \qquad \text{on } D_2 \tag{26b}$$

where

$$\phi_{\mathrm{ex}1} = -\int_{D_2} G_{12}\rho_{s2}\, ds \qquad \text{on } D_1 \tag{27a}$$

$$\phi_{\mathrm{ex}2} = -\int_{D_1} G_{21}\rho_{s1}\, ds \qquad \text{on } D_2. \tag{27b}$$

ρ_{s1} and ρ_{s2} are the charge densities on the striplines D_1 and D_2, respectively, in the absence of the other line.

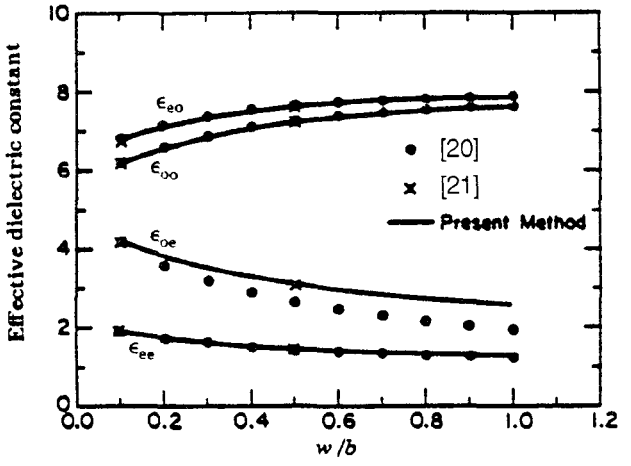

Fig. 9. Effective dielectric constants of the broadside, edge-coupled microstrip with inverted dielectric shown in Fig 3; $s/b = d/b = 0.2$, $t/b = 0$, $c/b = 10$, and $\epsilon_r = 10$.

The excess charge densities are solved by the iterative algorithm, and the equivalent capacitance can be defined similar to the one for the microstrip discontinuity. Hence, the equivalent capacitances for the orthogonal striplines can be expressed as

$$\Delta C_1 = \int_{S_{11}} \rho_{s\,ex1}\, ds + \int_{S_{12}} \rho_{s1}\, ds \text{ for strip line } D_1 \quad (28a)$$

$$\Delta C_2 = \int_{S_{21}} \rho_{s\,ex2}\, ds + \int_{S_{22}} \rho_{s2}\, ds \text{ for strip line } D_2 \quad (28b)$$

where S_{11}, S_{12}, S_{21}, and S_{22} are the regions bounded by the planes P_{11}, P_{11}, T_{11}, T_{12}, P_{21}, P_{22}, and T_{21}, T_{22}, respectively. Numerical results for the excess charge of two equal-width orthogonal strip lines for both even and odd excitations will be presented in the next section.

VII. Numerical Results

Numerical results for the MMIC structures discussed above will now be presented. The iterative scheme employed to derive the results is based upon an improved iterative approximation to the solution of the functional equations discussed in [14]. The iterative procedure is terminated when the boundary condition error (BCE) [15], [19] is smaller than 1×10^{-4}, or 0.01 percent. This iterative procedure is very efficient and only a few iterations are required for all the structures analyzed in this paper.

To illustrate the numerical efficiency of the iterative algorithm, let us first consider the broadside, edge-coupled, symmetric strip transmission line shown in Fig. 3. The spectral Green's function for this structure is constructed and modified according to (14) and (18), respectively. Due to the rapid decay of the product of the spectral Green's function and the magnitude square of the transform of the rectangular-pulse basis function away from $\alpha = 0$, the summation index m in (18) is chosen to be zero. This modified spectral Green's function is substituted into (17) and is solved iteratively using a 512-point FFT. The effective dielectric constants for the four propagating modes that

$$C = \begin{bmatrix} 8.53\times10^{-10} & -1.27\times10^{-11} & -2.06\times10^{-12} & -4.92\times10^{-13} & -1.58\times10^{-13} \\ -1.27\times10^{-11} & 8.53\times10^{-10} & -1.27\times10^{-11} & -2.05\times10^{-12} & -4.92\times10^{-13} \\ -2.06\times10^{-12} & -1.27\times10^{-11} & 8.53\times10^{-10} & -1.27\times10^{-11} & -2.06\times10^{-12} \\ -4.92\times10^{-13} & -2.05\times10^{-12} & -1.27\times10^{-11} & 8.53\times10^{-10} & -1.27\times10^{-11} \\ -1.58\times10^{-13} & -4.92\times10^{-13} & -2.06\times10^{-12} & -1.27\times10^{-11} & 8.53\times10^{-10} \end{bmatrix} F/m$$

Fig. 10 The Maxwell coefficient of capacitance for a five-line structure.

TABLE I
Average Number of Iterative Steps Required for the Ten Data Points Shown in Fig. 9 for Each of the Propagating Modes and Dielectric Constants

mode	$\varepsilon_r = 10$	$\varepsilon_r = 1$
	avg no. of iterations	avg no. of iterations
ee	5.2	5.3
eo	4 6	4.7
oe	6.2	4.9
oo	4 6	4.8

TABLE II
Reduction of BCE and Calculated Capacitance by Retaining a Different Number of Sample Points of the Approximated Spatial Green's Function

no. of iterations	BCE(%) FFT SIZE			
	1024	512	256	128
0	100	100	100	100
1	6 6	6.6	6 6	6.6
2	0.031	0.031	0.031	0.031
3	0.0027	0.0027	0.0027	0.0026
4	0.00014	0.00014	0.00014	0.00014
C (nF / m)	0.4317	0.4317	0.4317	0.4315

can be supported by this transmission line are plotted in Fig. 9. Each of these curves consists of ten data points and each data point requires two solutions from (17), one for $\epsilon_{r2} = 1$ and one for $\epsilon_{r2} = 10$. It took 7.147 s on a Cray X-MP/48 supercomputer to generate these curves by solving (17) 80 times. The minimum number of iterations required is three whereas the maximum is nine. The average iterative steps required for the ten data points for each of the propagating modes and dielectric constants are listed in Table I. The calculated effective dielectric constants agree very well with those presented in [20] and [21], except for the odd–even mode. For this mode, we confirm the findings of [21] that the symmetric charge distribution used in [20] is a poor approximation; this is evident from the excellent agreement between or results and those in [21]. It should be noted that if the BCE for this problem is set at 0.1 percent instead of 0.01 percent, the calculated effective dielectric constants will remain relatively unchanged although the number of iterations and hence the CPU time can be reduced significantly. The numerical efficiency of the iterative algorithm and the numerical treatment of the spectral Green's function have been demonstrated for this periodic problem.

Next, let us turn our attention to the aperiodic one. The multiconductor transmission line, as shown in Fig. 4, is

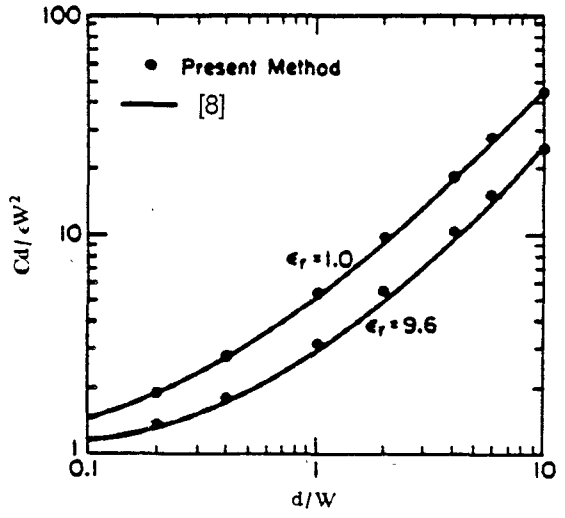

Fig. 11. The normalized capacitance of the square microstrip patch shown in Fig. 5.

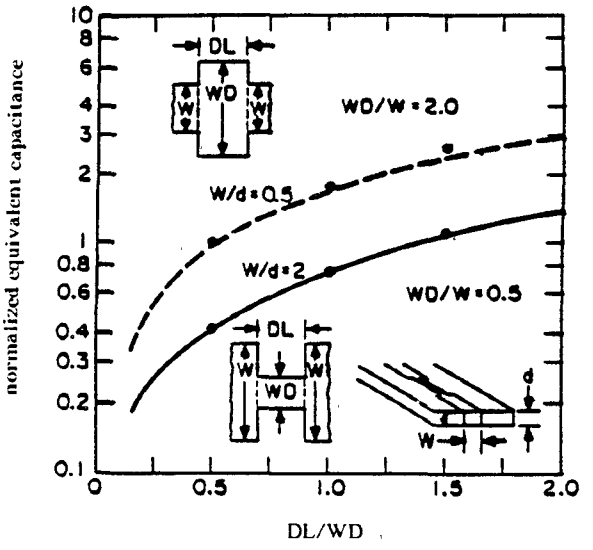

Fig. 13. Normalized equivalent capacitance for a double step discontinuity. • present method; --- [13].

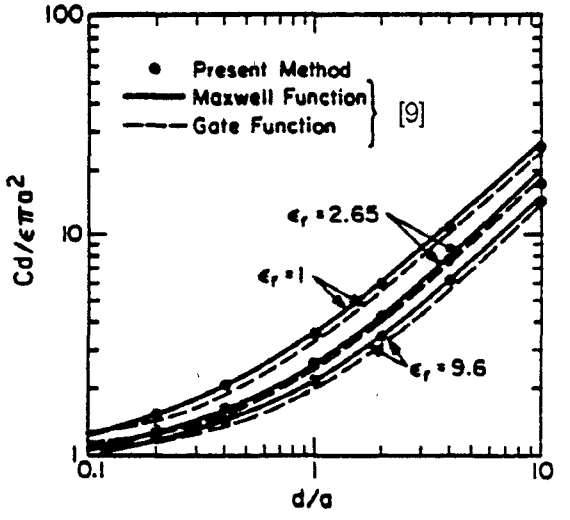

Fig. 12. The normalized capacitance of the circular microstrip patch shown in Fig. 5.

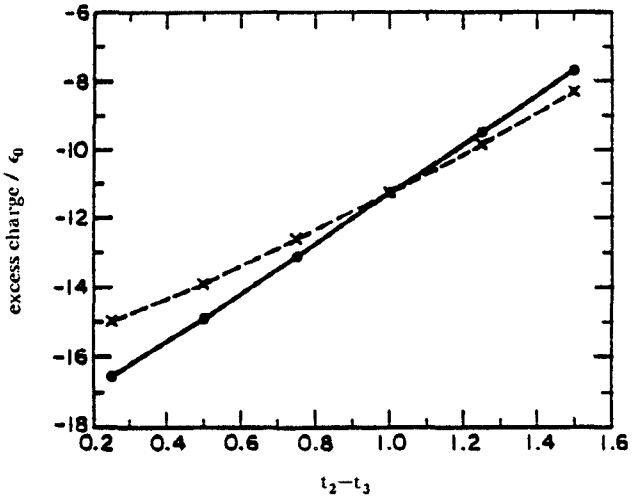

Fig. 14. Normalized excess charge on the orthogonal striplines shown in Fig. 8 for an even excitation. ——top strip; ---- bottom strip; $t_1 = 3$, $t_3 = 1$, $w = 1$, and $\epsilon_r = 4.5$.

analyzed at a frequency of 16 MHz. To approximate this aperiodic problem, van den Berg chose a period of 50 times the width of one strip [15]. Assuming we have only two conducting strips and there are 18 sample points on each strip, a 1024-point FFT is required. However, if the approximation of the spectral Green's function discussed in Section IV-B is used, only a 128-point FFT is necessary, and a considerable saving in computation time is realized. Table II shows the reduction of BCE as well as the capacitance for the two conducting strips when the parameters shown in [15, table III] are used. Although not shown here, the charge distribution computed by using the spectral Green's function with 1024 sample points is essentially the same as those obtained with the modified Green's function with 512, 256, or 128 points. As shown in Table II, the capacitances calculated by using these distributions are in very close agreement with each other. It should be noted that the charge density is updated for each iteration in this paper, and is not evaluated from the potential function in the final step, as in [15]. The Maxwell coefficient of capacitance of a five-line structure is given in Fig. 10. To avoid the problem of singularity of the spectral Green's function at $\alpha = 0$ [15], a ground plane is introduced into the Si layer to make it 10 μm thick. Each conducting strip has 18 sample points and a 512 FFT is employed. The BCE reduces to less than 0.01 percent in three iterations for all five independent excitations. The accuracy of the solution can be readily improved by increasing the number of sample points on the strips.

For the computer-aided design of three-dimensional planar MMIC structures, we first need to generate the modified spectral Green's function discussed in Section IV-B. To carry out an inverse FFT of the sampled spectral Green's function on a 512×512 grid requires about 6 s on the Cray X-MP/48. However, if we initially generate a data base for each dielectric thickness and dielectric constant, we can subsequently use this modified Green's func-

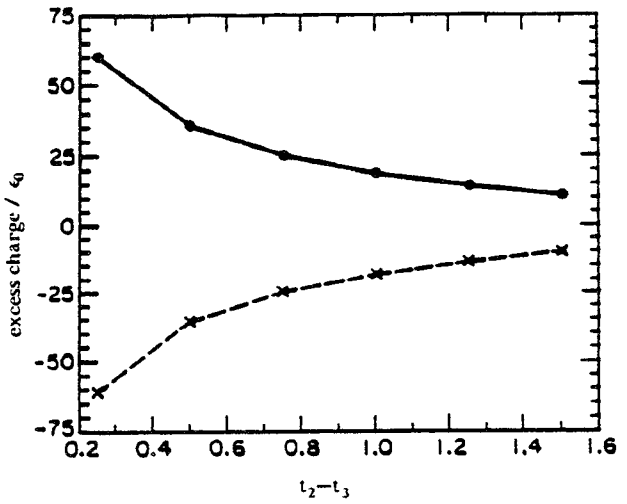

Fig. 15. Normalized excess charge on the orthogonal strip lines shown in Fig. 8 for an odd excitation. ——— top strip; ---- bottom strip; $t_1 = 3$, $t_3 = 1$, $w = 1$, and $\epsilon_r = 4.5$.

tion data to analyze either an arbitrarily shaped patch or a microstrip discontinuity. Figs. 11 and 12 show the normalized capacitances for square and a circular patches, respectively. Using the data from the Green's function data base, it takes only three iterations and about 0.3 s for each of the data points when a 32×32 FFT is employed. Excellent agreements with the results in [8] and [9] are obtained.

Fig. 13 shows the normalized equivalent capacitance for a double step discontinuity. Good agreements with the results in [13] are obtained. In this structure, a 64×64 FFT is used and it requires only three iterations. It should be noted that when the ratio of the length to the width of the discontinuity increases, a larger FFT size is required and the iterative procedures become less efficient. Figs. 14 and 15 show the variations of the normalized excess charge on two orthogonal strip lines with strip separation. Fig. 14 shows the excess charge on the top and bottom strips for an even excitation, whereas the corresponding results for the odd excitation appear in Fig. 15. For the even excitation, the excess charges on the two strips are equal at $t_2 = 2$, because the orthogonal strip lines are symmetric for this value. For the odd excitation, the excess charges are always equal and opposite.

VIII. Conclusions

A class of MMIC structures has been analyzed in this paper using as numerically rigorous iterative procedure. The transfer-matrix method is employed for the problem of deriving the spectral Green's functions for a multilayered structure because of the convenience with which the method can be applied to this problem. The periodic nature of MMIC structures surrounded by electric side walls allows one to achieve numerical efficiency via the use of the FFT. For the periodic problem, a numerical procedure for treating the Green's function, which has an infinite support in the spectral domain, is discussed. This treatment enables one to use the FFT with only a finite number of points. On the other hand, further approximation yields reasonably good spatial Green's functions, as evident from the numerical results, such that an FFT of much smaller size can be used for the aperiodic problem. For all the structures discussed in this paper, the boundary condition error reduces to a level below 0.01 percent within a few iterations. This leads us to conclude that the iterative approach described in this paper is well suited for MMIC design.

References

[1] H A. Wheeler, "Transmission-line properties of parallel strips separated by a dielectric sheet," *IEEE Trans. Microwave Theory Tech* , vol. MTT-13, pp. 172–185, Mar 1965.

[2] T. G. Bryant and J. A. Weiss, "Parameters of microstrip transmission lines and of coupled pairs of microstrip lines," *IEEE Trans. Microwave Theory Tech.*, vol. MTT-16, pp. 1021–1027, Dec. 1968.

[3] E. Yamashita and R. Mittra, "Variational method for the analysis of microstrip lines," *IEEE Trans. Microwave Theory Tech.*, vol. MTT-16, pp. 251–256, Apr 1968.

[4] Y Rahmat-Samii, T. Itoh, and R. Mittra, "A spectral domain technique for solving coupled microstrip line problems," *Arch. Elek. Übertragung.* Band 27, pp. 69–71, Feb 1973

[5] W. T. Weeks, "Calculation of coefficients of capacitance of multiconductor transmission lines in the presence of a dielectric interface," *IEEE Trans. Microwave Theory Tech.*, vol. MTT-18, pp. 35–43, Jan. 1970.

[6] C. Wei, R. F. Harrington, J. R. Mautz, and T. K. Sarkar, "Multiconductor transmission lines in multilayered dielectric media," *IEEE Trans. Microwave Theory Tech.*, vol. MTT-32, pp. 439–450, Apr. 1984.

[7] R. F. Harrington and C. Wei, "Loss on multiconductor transmission lines in multilayered dielectric media," *IEEE Trans. Microwave Theory Tech.*, vol. MTT-32, pp. 705–710, July 1984.

[8] T. Itoh, R. Mittra, and R. D. Ward, "A method for computing edge capacitance of finite and semi-infinite microstrip lines," *IEEE Trans. Microwave Theory Tech.*, vol. MTT-20, pp. 847–849, Dec. 1972.

[9] T. Itoh and R. Mittra, "A new method for calculating the capacitance of a circular disk for microwave integrated circuits," *IEEE Trans. Microwave Theory Tech.*, vol. MTT-21, pp. 431–432, June 1973.

[10] S. R. Borkar and R. F. H. Yang, "Capacitance of a circular disk for application in microwave integrated circuits," *IEEE Trans. Microwave Theory Tech.*, vol. MTT-23, pp. 588–591, July 1975.

[11] W. C. Chew and J. A. Kong, "Effects of fringing fields on the capacitance of circular microstrip disk," *IEEE Trans. Microwave Theory Tech.*, vol. MTT-28, pp. 98–104, Feb. 1980.

[12] P Silvester and P Benedek, "Microstrip discontinuity capacitances for right-angle bends, T-junctions and crossings," *IEEE Trans. Microwave Theory Tech* , vol MTT-21, pp. 341–346, May 1973.

[13] P Anders and F. Arndt, "Microstrip discontinuity capacitances and inductances for double steps, mitered bends with arbitrary angle, and asymmetric right-angle bends," *IEEE Trans. Microwave Theory Tech.*, vol. MTT-28, pp. 1213–1217, Nov. 1980.

[14] P. M van den Berg, "Iterative schemes based on the minimization of the error in field problems," *Electromagnetics*, vol. 5, nos. 2–3, pp 237–262, 1985.

[15] P. M. van den Berg, W Ghijsen, and A. Venema, "The electric-field problem of an interdigital transducer in a multilayered structure," *IEEE Trans. Microwave Theory Tech.*, vol MTT-33, pp. 121–129, Feb. 1985

[16] C H Chan and R. Mittra, "Analysis of a class of cylindrical multiconductor transmission lines using an iterative approach," *IEEE Trans. Microwave Theory Tech* , vol MTT-35, Apr. 1987.

[17] F. Medina and M Horno, "Upper and lower bounds on mode capacitances for a large class of anisotropic multilayered microstrip-like transmission lines," *Proc. Inst. Elec. Eng* , vol. 132, pt. H, pp. 157–163, June 1985.

[18] A. F. Peterson, "An analysis of the spectral iterative technique for electromagnetic scattering from individual and periodic structures," *Electromagnetics*, vol. 6, no. 3, pp 255–276, 1986.

[19] C. H. Chan and R. Mittra, "On the analysis of frequency selective surfaces using subdomain basis functions," *IEEE Trans. Antennas Propagat.*, to be published.

[20] S. K. Koul and B. Bhat, "Broadside, edge-coupled symmetric strip transmission lines," *IEEE Trans. Microwave Theory Tech.*, vol. MTT-30, pp. 1874–1880, Nov. 1982.
[21] B. Climer, "Modes on a four-conductor line," *Inst. Elec. Eng.*, vol. 133, pt. H, pp. 392–394, Oct 1986.
[22] T. Kitazawa, private communications.

✠

Chi Hou Chan (S'86–M'87) was born in Macao on April 16, 1959. He attended Hong Kong Polytechnic and the City College of New York. He received the B.S. and M.S. degrees in electrical engineering from the Ohio State University, Columbus, in 1981 and 1982, respectively, and the Ph.D. degree in electrical engineering from the University of Illinois, Urbana, in 1987.

From 1981 to 1982, he was a Graduate Research Associate at the ElectroScience Laboratory, Ohio State University. Since August 1982, he has been with the Electromagnetic Communication Laboratory in the Department of Electrical and Computer Engineering at the University of Illinois, where he is presently a Visiting Assistant Professor. His research interests include numerical techniques in electromagnetics, scattering from electrically large bodies, frequency-selective surfaces, microwave integrated circuits, high-speed digital circuits, and integrated optics.

✠

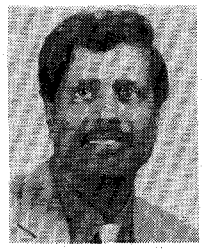

Raj Mittra (S'54–M'57–SM'69–F'71) is the Director of the Electromagnetic Communication Laboratory of the Electrical and Computer Engineering Department and Research Professor of the Coordinated Science Laboratory at the University of Illinois. he is a Past-President of AP-S. He serves as a consultant to several industrial and governmental organizations in the United States.

His professional interests include the areas of analytical and computer-aided electromagnetics, high-speed digital circuits, radar scattering, satellite antennas, microwave and millimeter wave integrated circuits, frequency selective surfaces, EMP and EMC analysis, and interaction of electromagnetic waves with biological media.